Published in final edited form as:
Nat Neurosci. 2009 April ; 12(4): 492–501. doi:10.1038/nn.2283.

Phase-to-rate transformations encode touch in cortical neurons of a scanning sensorimotor system

John C Curtis[1,2,4] and **David Kleinfeld**[2,3]

[1]Division of Biological Sciences, University of California, San Diego, California, USA.

[2]Computational Neurobiology Graduate Program, University of California, San Diego, California, USA.

[3]Department of Physics, University of California, San Diego, California, USA.

Abstract

Sensory perception involves the dual challenge of encoding external stimuli and managing the influence of changes in body position that alter the sensory field. To examine mechanisms used to integrate sensory signals elicited by both external stimuli and motor activity, we recorded from rats trained to rhythmically sweep their vibrissa in search of a target. We found a select population of neurons in primary somatosensory cortex that are transiently excited by the confluence of touch by a single vibrissa and the phase of vibrissa motion in the whisk cycle; different units have different preferred phases. This conditional response enables the rodent to estimate object position in a coordinate frame that is normalized to the trajectory of the motor output, as defined by phase in the whisk cycle, rather than angle of the vibrissa relative to the face. The underlying computation is consistent with gating by an inhibitory shunt.

The perception of object location relative to the body depends on tracking sensor position—eyes for seeing or fingers for touching—as much as on the activation of those sensors by features of an object. Over a half century ago, von Holst[1] emphasized that one cannot hope to understand sensation without consideration of the effects "produced on the sensory-receptors by the motor impulses which initiate a muscular movement." von Holst factored the signals required for sensation into three components. One is an afferent signal that originates from environmental influences—for example, light for the case of looking and pressure for the case of touching—and is denoted ex-afference. A second component is an afferent signal that results from activation of sensory receptors by self-motion and is called reafference. The motor-driven sensory input can involve the same receptors that encode external stimuli, as in the case of peripheral reafference, or a separate group of receptors, as in the case of proprioception. A final sensory component may be provided by an efference copy of the motor command; this corresponds to the intended rather than actual motor activation of sensory receptors. The ex-afferent component can interact with one or both motor signals (that is, reafference or efference copy) to produce a perceptually stable representation of the identity and location of external stimuli relative to a changing body configuration.

Correspondence should be addressed to D.K. dk@physics.ucsd.edu.
[4]Present address: Systems Neurobiology Laboratory, The Salk Institute for Biological Studies, San Diego, California, USA.

Supplementary information is available on the Nature Neuroscience website.

The coexistence and possible interaction of ex-afference, reafference and efference copy signals has been demonstrated from peripheral to thalamocortical levels[2]. In gaze control, reafferent signals of actual eye position and efference copy of the intended position of gaze3 gate the input to vestibular nuclei as part of the vestibular ocular response4. In the visual system, neurons in cat thalamus5 and primary visual cortex[6] respond to visual stimuli (the ex-afferent signal) and to the stimulation of extra-ocular muscle proprioceptors (a reafferent signal). Further, interactions between ex-afference visual signals and a presumed reafference of eye position have been observed at multiple levels of cortical processing in primates[7]. Responses to combinations of ex-afference, reafference and efference copy signals lie at the heart of transformations to place sensory input in body-centered coordinates. Yet mechanistic and conceptual understandings of how ex-afference and reafference interact to generate such transformations are lacking.

Rats sweep their vibrissae through space with stereotypical rhythmic motions as they locomote and search for objects in their immediate environment. Multiple features of the rat vibrissa system make it an ideal nervous system for studying the interaction of ex-afference and reafference. First, behavioral work has shown that rats can determine the position of an object relative to that of its head through the use of a single moving vibrissa[8]. This implies that the underlying computation of touch in a head-centered coordinate system depends on the interaction of an ex-afference signal (that is, vibrissa contact) with either a reafference or an efference copy that reports vibrissa position. A substrate for such interactions is provided by anatomical connections among sensory and motor areas, at the levels of brainstem through cortex[9,10], that form nested feedback loops11,12. Efferent signals give rise to rhythmic motor activity that results in stereotypical whisking behavior13. This motion in turn generates a robust peripheral reafference that is locked to the phase of the vibrissae in the whisk cycle[14] and strongly modulates the output of neurons in vibrissa primary sensory (S1) cortex[15–17], with different neurons having different preferred phases15. Recent evidence suggests that reafference and ex-afference signals are communicated along parallel pathways from the brainstem to cortex18,[19]. Thus ex-afferent and reafferent signals associated with vibrissa-based touch are likely to remain separate until they are allowed to interact in vibrissa S1 cortex.

Here, we test the hypothesis that ex-afference touch signals are modulated by reafference signals associated with sensor motion to form a representation of object location relative to the animal's body plan. We ask the following questions: first, what is the nature of ex-afferent vibrissa touch signals encoded by single units in vibrissa S1 cortex? Past results consider only responses that are induced by passive rather than active vibrissa movement. Second, is touch represented in a coordinate system that is matched to the region currently scanned, defined by the phase of the vibrissa in the whisk cycle, or one that spans the full range of vibrissa position? Past results[15–17] imply that the reafferent signal encodes phase, which suggests but does not establish that touch is also encoded in terms of phase. Finally, how can known cortical circuits give rise to the observed interaction of ex-afferent and reafferent signals?

RESULTS

Rats were trained to palpate a sensor with their vibrissae in either a free-ranging (Fig. 1a) or a body-constrained (Fig. 1b) behavioral configuration. In both paradigms, whisking was accompanied by large movements of the head, so that contact of a vibrissa with the sensor spanned all possible phases of the whisk cycle (Supplementary Fig. 1 online); there was a small but significant ($P < 0.01$) excess of touch events at protraction over retraction. Animals that succeeded in this task underwent surgery to implant a microwire head stage[20] above vibrissa S1 cortex to record broadband electrical activity. These signals were

subsequently sorted into single units[21], as verified by the consistency of spike waveforms across instances and autocorrelation functions that decay toward zero at equal time (Fig. 1c). We established the principal vibrissa[22] for each of two to four electrodes in S1 cortex and trimmed all but these vibrissae; no systematic differences in whisking or touch were observed that were related to different numbers of intact vibrissae. Further, microwires were implanted into the mystacial pad to record the differential electromyogram (∇EMG) of the muscles that drive the vibrissa motion.

The rectified ∇EMG was used to deduce the phase of the vibrissae, denoted $\phi(t)$, during contact events and during periods of time when rats were coaxed to whisk freely in the air[16]. These epochs of free-whisking13 allowed the reafferent response to whisking to be assessed (Fig. 1d and Supplementary Fig. 2 online). Videographic imaging was used to deduce the phase and angular position, $\theta(t)$, of the vibrissae surrounding contact events, and to confirm that only a single vibrissa touched the sensor (Fig. 1c). The resulting spike, ∇VEMG data, videographic data and touch sensor signals were sufficient to calculate the spiking as a function of phase in the whisk cycle during free whisking as well as spiking as a function of both phase and absolute angle during epochs of vibrissa contact (Fig. 1d and Supplementary Fig. 2).

The instantaneous phase in the whisk cycle is denoted $\phi(t)$; this can be expressed as $\phi(t) = [2\pi f_{whisk} t - \phi_{whisk}]_{modulo\ 2\pi}$ during rhythmic whisking, where f_{whisk} is the whisking frequency and ϕ_{whisk} is the preferred phase. A preferred phase of $\phi_{whisk} = 0$ corresponds to the protracted position, $\phi_{whisk} = \pm\pi$ is the retracted position, and negative (positive) angles indicate protraction (retraction). The instantaneous angular position and phase are related by $\theta(t) = \theta_{midpoint}(t) + \Delta\theta(t) \cdot \cos[\phi(t)]$, when the midpoint, $\theta_{midpoint}(t)$, and amplitude, $\Delta\theta(t)$, vary only slowly on the timescale of the period of whisking, that is, $1/f_{whisk}$.

Single units respond during free whisking as well as touch

We recorded 152 single units in the vibrissa S1 cortex of nine rats, a majority of which responded to whisking in free air. No differences were seen between free-ranging (Fig. 1a) versus body-constrained (Fig. 1b) paradigms. Cross-correlations between spiking activity and the rectified ∇EMG show that individual units tend to spike at specific phases of the whisk cycle (Fig. 2a–d, left column). The presence of units whose spike rate remains phasically modulated in time follows from the narrow distribution of whisking frequencies[13] (f_{whisk} = 8.7 ± 1.3 Hz; mean ± s.d.). In an extension of past work, we found that the spike rate during free whisking epochs appears unchanged from that during periods of negligible mystacial ∇EMG activity, such as when an animal walks without whisking (Fig. 2e). Thus whisking tends to reorganize the timing of spikes rather than add new spikes, which is reminiscent of the effect of finger taps on the response of neurons in the primary somatosensory area of monkeys[23].

Most single units responded to active touch (Fig. 2a–d, middle column). Three broad classes of responses emerged based on trial-averaged responses: rapid excitation (Fig. 2a), slow net inhibition (Fig. 2b) similar to that seen under nonwhisking conditions[24] and slow net excitation (Fig. 2c). The temporal delineation between rapidly and slowly responding cells was sharp (Supplementary Fig. 3 online), and all classes of neurons contained both narrow and broad spike waveforms[25] (Supplementary Fig. 4 online). Rapidly excited units responded to touch with phasic spiking that had a latency to onset of 5 to 9 ms and ranged from 12 to 44 ms in duration. These units had the greatest maximum spike rate (Fig. 2f) and fired about 2% of their action potentials in bursts (Supplementary Fig. 5 online). They were largely confined to the granular and deep infragranular layers (Fig. 2g and Supplementary Fig. 6 online), which is consistent with data gathered from anesthetized animals in which whisking was driven by electrical stimulation of the vibrissa motor nerve[18,26]. Both

categories of slowly responding neurons encode the behavioral task *per se* (as well as touch) in that their spike rates change as the rat cranes and whisks vigorously as it attempts to touch the sensor (Fig. 2c, middle row). Neurons that exhibited slow excitation upon touch dominated the supragranular and infragranular layers, whereas those with slow inhibitory responses were uniformly distributed among all layers (Supplementary Fig. 6).

Phase in the whisk cycle gates the rapid touch response

We observed that 20% of the single units were both rapidly excited by touch and modulated by whisking. These units, designated as RE touch/whisking neurons, form the locus of our analysis on the confluence of ex-afferent touch and reafferent whisking signals. Our goal was to test whether the touch responses were modulated by the phase of the vibrissa in the whisk cycle at the time of contact. We illustrate the analysis process in terms of the data for three example units whose preferred phases span the full range of whisking (Fig. 3a–d). First, we fit sinusoids to the rectified ∇EMG signal surrounding each contact event as a means to model rhythmic whisking and determine the phase in the whisk cycle at the time of contact (Fig. 3a). Second, a smooth rate function was fit to the event-averaged touch response for each unit (Fig. 3b). Third, individual touch responses were sorted into one of eight phase intervals within the whisk cycle. The average touch response within each phase interval was fit as a scaled version of the previously derived smooth rate function for that neuron (Fig. 3c); we note that the shape of the touch response appeared invariant to amplitude. Finally, the peak amplitude of the eight fitted functions defined a tuning curve of touch response versus phase in the whisk cycle (Fig. 3d).

We observed that the touch response for each unit is strongly modulated by vibrissa position, such that the response is maximal at or near the preferred phase during free whisking (compare panels in Fig. 3a with those in Fig. 3d); this is highlighted when the spike response is visualized on a logarithmic scale (Fig. 3e). There is no systematic change in the amplitude of whisking as a function of where contact occurs in the whisk cycle (Supplementary Fig. 7 online). The maximum spike rate for the response to touch is about tenfold higher, on average, than the approximately 9-Hz average spike rate during whisking. The strong modulation of the touch response is suggestive of a nonlinear interaction between reafference and ex-afference.

In general, RE touch/whisking units showed responses to touch that were tuned to the phase of the whisk cycle (28 of 35 units) (all responses in Supplementary Figs. 8 and 9 online). A summary shows that the phase at the maximal touch response for each unit, denoted as ϕ_{touch} (Fig. 3d), is statistically equal to the unit's preferred phase during free whisking; that is, $\phi_{touch} \approx \phi_{whisk}$ (Fig. 4a). All values of preferred phase are represented, with a distribution that is biased toward retraction (Fig. 4a, side bars). All tuning curves are relatively broad, with an average half width at half maximum of $0.32\pi \pm 0.05\pi$ radians (mean ± s.d.) (Fig. 4b, thick line); this coincides with the $\pi/3$ radian width for cosine-shaped tuning curves.

We next determined whether the spike rate during free whisking is predictive of the peak rate upon touch. In contrast to naïve expectations, the maximum rate upon touch was nearly independent of the average spike rate during free whisking ($P = 0.05$) (Fig. 4c). A related analysis considers the modulation depth of the spike rates (Fig. 4d, inset)

$$\text{Modulation depth} \equiv \frac{\text{Maximum spike rate} - \text{Minimum spike rate}}{\text{Mean spike rate}} \quad (1)$$

The modulation depth of the tuning curve for the touch response was, on average, four times greater than that for the free whisking response. Neither the spike rate nor the modulation

depth showed a systematic dependence on preferred phase in the whisk cycle (Supplementary Fig. 10 online). Critically, the modulation depth for touch at different phases in the whisk cycle was statistically independent ($P = 0.8$) of the modulation of the rate during free whisking (Fig. 4d).

Vibrissa angle is a poor modulator of the touch response

We revisited the possibility that the spike response upon contact may be a function of angular position, which depends on the midpoint angle and amplitude of the whisk, in addition to phase in the whisk cycle (Fig. 4a,b). Position data were derived from videographic images during contact events (Fig. 1c). As a control, we compared the phase of the vibrissae in the whisk cycle at the time of contact derived from the videographic data (Fig. 5a,b and Supplementary Fig. 8) with the phases derived from the ∇EMG data. The two sets of data closely match (Supplementary Fig. 11 online). We next considered modulation in the spike rate upon contact as a function of position (Fig. 5c,d) and observed a relatively small and insignificant modulation.

The modulation of the touch response by phase in the whisk cycle was relatively high: an average of 1.2 across the 2π radian range of phase (Fig. 5e). In contrast, the modulation of the touch response by position averaged only 0.4 across the full range of whisking angles and was statistically significant ($P < 0.05$) in only 14% of the cases (Fig. 5f). As an average over all RE touch/whisking units, the amplitude of whisking varied by 12° between trials, or 70% of the average value of $\Delta\theta$, whereas the midpoint of the region of whisking varied by 6° between trials, or 35% of the average amplitude (Fig. 5g). In summary, RE touch/whisking units encode touch in terms of phase, which is normalized to the particular amplitude and midpoint, as opposed to angular position, on a given trial.

We consider the possibility that the broad tuning curve for the touch response as a function of phase in the whisk cycle (Fig. 4b) results from a preferred phase, ϕ_{touch}, that is modulated by the amplitude or the frequency of whisking. Under these contingencies, the observed broad curve could be the sum of multiple narrow curves, each with a slightly different value of ϕ_{touch}. For the example of unit three (Figs. 3 and 5), we observe no difference in either the preferred phase ϕ_{whisk} or the width of the tuning curve when the dataset is equally divided based on trials with large-amplitude versus small-amplitude whisks (Fig. 6a–c). A similar invariance occurs when the dataset is equally divided based on trials with lower versus higher whisking frequencies (Fig. 6a,d,e), for which time delay could in principle lead to a frequency-dependent phase. Signal-to-noise constraints allowed us to perform this analysis for only 6 of the 28 RE touch/whisking units, yet all showed statistically significant invariance ($P < 0.02$) with regard to preferred phase and broad tuning (Supplementary Fig. 12 online).

DISCUSSION

Active sensing by the rat vibrissa system involves two sensory signals: a reafferent signal of motor activity that encodes the phase of the vibrissa in the whisk cycle and an ex-afferent signal that encodes touch (Fig. 2). We have shown that these two signals are merged in a highly nonlinear manner (Figs. 3 and 4) in vibrissa S1 cortex and that contact is coded with respect to vibrissa phase rather than angular position (Fig. 5). The coding is robust and invariant with respect to changes in whisking parameters (Fig. 6).

The representation of contact in a normalized, relative coordinate system that is dynamically generated by the motor trajectory is somewhat similar to the coding of visual stimuli in dynamic, objected-centered coordinates, as occurs in parietal and premotor cortices in primates[7,27]. This is in contrast to the static, retinotopic coordinates instantiated by primary

visual areas. Coding in phase coordinates implies that there is a common pathway for the reafferent and ex-afferent signals, or that these signals follow separate pathways with similar adaptation. To the extent that separate pathways are used, as has been suggested[18], we propose a neuronal circuit that computes the location of objects within a sensory field (Fig. 7a).

Origin of the reafferent signal

A reafference signal that encodes the phase in the whisking cycle is present at the level of primary sensory neurons in the trigeminal ganglion14,28. In animals that whisk (for example, mice, rats and gerbils), vibrissa follicles are innervated with both deep and superficial nerve endings[29]. Both innervations are distinct and highly structured, and they terminate in different regions of the trigeminal complex. Notably, animals that do not whisk (for example, cats, guinea pigs and rabbits) either completely lack superficial follicle receptors or the innervation is sparse and largely unstructured. This led to the hypothesis that superficial nerve innervation serves as proprioceptive reafference for vibrissa motion29. The mechanism by which compression of the follicle during movement is transformed into a phase code is unknown, but it could involve adaptation to the range of whisking30.

A second issue involves the possibility that the reafference and ex-afference form separate thalamocortical tracks19. There are four pathways—one that involves posterior medial thalamus and three that involve subdivisions of ventral posterior medial thalamus—that originate from different populations of secondary sensory cells in the trigeminal nuclei[31]. Recent reports provide evidence (albeit controversial) that the posterior medial thalamic pathway encodes predominantly vibrissa motion[18,32], whereas at least one of the ventral posterior medial thalamic pathways encodes predominantly touch18.

Model for the interaction of contact and whisking signals

A biophysical model for gating of the active touch response must account for four phenomena. First, the ex-afferent touch signals and the reafferent free whisking responses are enhanced at the same phase in the whisk cycle (Fig. 4a). Second, the spike rate amplitudes and modulation depths of the spike rates for touch and free whisking responses are independent (Fig. 4c,d). Third, the modulation of the touch response is much greater than the relatively small modulation of the spike rate by free whisking (Figs. 2d and 4c,d). Fourth, the whisking reafference essentially does not change the background spike rate (Fig. 2e).

Summation of the ex-afferent and reafferent inputs, followed by a spike-generating mechanism whose firing rate is a steeply increasing function of input current, is a potential mechanism for the observed phenomena. However, a substantial increase in the slope of spike rate versus input current is unprecedented for cortical neurons[33]. A related scheme makes use of the summation of signals near threshold[33]. However, both whisking and touch events ride on a substantial background rate for all of our units (Figs. 2–4). Multiplication of the ex-afferent touch signal with the reafferent whisking signal is a potential nonlinearity that can strongly modulate the touch response by the phase in the whisk cycle. One expectation for this scheme that is implicit from studies on the multiplication of signals by neurons[34–37] is that the amplitude of the touch response should track that of the whisking response. However, in contrast to this expectation, the modulation depth for touch at different phases in the whisk cycle was independent of the modulation of the rate during free whisking (Fig. 4d).

We propose that shunting inhibition of a putative touch pathway by a whisking pathway provides a likely circuit to gate the touch response by the phase in the whisk cycle. Shunting

inhibition[38] also provides a means for one input to modulate the synaptic gain of a second input. A minimal model consists of a neuron with three compartments, each with a leak battery with resistance R and potential E_L, arranged so that (i) an active zone has a bias battery, with conductance G_B and potential E_B, and generates spikes; (ii) a soma receives shunting—that is, $GABA_A$-mediated synaptic input with a battery with conductance G_S and inhibitory potential E_S, where $E_S \sim E_L$; and (iii) a dendritic compartment receives excitatory synaptic input with a battery with conductance G_E and excitatory potential E_E (Fig. 7a). The sequential arrangement of the compartments, taken for simplicity to be one electrotonic length apart, allows the inhibitory whisking input to both modulate the background spike rate and gate an excitatory touch input (Figs. 2a and 3). Putative inhibitory neurons that are strongly modulated by whisking but not touch in close proximity to rapidly excited touch cells is consistent with our laminar analysis of different classes of single units (Fig. 2g and Supplementary Fig. 6).

Insight into the mechanism of shunting inhibition can be gleaned from a linear analysis of the circuit because the spike rate tracks the membrane potential in the presence of high background activity[39]. For simplicity, we ignore the bias current and assume that the maximal synaptic conductances are large (Fig. 7a). Contact at the preferred phase in the whisk cycle, that is, $\phi = \phi_{whisk}$ so that $RG_S = 0$, leads to a membrane potential of $V_m \sim (4E_L + E_E)/5$ at the active zone, which exceeds the rest level $V_m \sim E_L$. In contrast, when contact occurs at $\phi = \phi_{whisk} \pm \pi$, so that $RG_S \gg 1$, the excitatory touch input is shunted by the inhibitory whisking input, and the membrane potential falls to $V_m \sim (E_L + E_S)/2 + E_E/(2RG_S)$, which is close to the rest level. The independence of touch and whisking is seen by estimating their modulation depths (equation (1)), with V_m as a surrogate for spike rates

$$\text{Modulation depth}\Big|_{\text{Whisking}} \simeq \frac{1}{4}\left|\frac{E_L - E_S}{E_L}\right| \xrightarrow[E_L \sim E_S]{} 0 \tag{2}$$

which approaches zero when the shunt and leak potentials are equal, and

$$\text{Modulation depth}\Big|_{\text{Touch}} \simeq \frac{2}{5}\left\{\frac{3(E_L - E_S) + E_E + \left|2E_S\right|}{\left|3E_L - E_S\right|}\right\} \xrightarrow[E_L \sim E_S]{} \frac{1}{5} \tag{3}$$

which approaches a constant in the same limit. Thus the modulation depth for touch can be both independent of that for whisking and larger, which is consistent with our observations (Fig. 4d).

Numerical analysis of the model (Fig. 7a) with a Hindmarsh-Rose– type mechanism for spike generation and parameters appropriate for cortical neurons[40] clearly shows that the response to touch is enhanced at the preferred phase in the whisk cycle (Fig. 7b,c). Simulations with different bias conductances show that whisking has only a marginal effect on the spike rate (Fig. 7d). Simulations with different shunt conductances show that the amplitude of the touch response is independent of the amplitude of the free whisking spike rate (Fig. 7e), and that modulation in the spike rate by changes in vibrissa position is both much greater than and independent of the modulation during free whisking (Fig. 7f). The proposed circuit can, in principle, be confirmed or refuted by recording the intracellular potential from layer 4 spiny stellate or star pyramidal cells in rats that are trained to whisk[17,41]. A combination of ion blockers and voltage clamping should reveal whether the whisking response is mediated by inhibitory input.

Spike rates and angular resolution

The average ongoing rate of spiking hovers around 9 Hz (Fig. 2e), and the average modulation of the spike rate by whisking *per se* is ± 2 spikes per second. This corresponds to ~0.4 spikes per whisk, on top of a fluctuating background of ~1 spike per whisk. We estimate that the output from ~200 neurons must thus be summed to achieve a resolution of π/3 radians, as set by the tuning curve (Fig. 4b), to specify the phase in the whisk cycle on a single trial basis. Decoding schemes that make use of the absence of a response at nonpreferred phases may lower this estimate. On the other hand, the consensus view of the spike rate of neurons in vibrissa S1 cortex is evolving, with evidence from intracellular studies that the ongoing rates for many neurons may lie closer to 1Hz than 10Hz[42,43]. A lower average rate would increase the variability and increase the estimate.

With regard to contact-induced spikes, active touch leads to an average, integrated response of 2 spikes per contact within a window of ~20 ms (Fig. 3b); this further coincides with the time spent in each resolvable phase interval of π/3 radians (Fig. 4b). The additional spikes generated by active touch substantially exceed the ~0.4 spikes generated by whisking alone and should be sensed with high fidelity. Resolution at a scale much finer than π/3 radians may be achieved by averaging the responses from multiple neurons. Finally, for the average whisking range of ±17° (Fig. 5g), the corresponding angular resolution is ~5°, which approximates the typical threshold for bilateral perceptual acuity with a vibrissa[44].

Relation to directional tuning

Directional tuning is a common metric used to quantify neuronal response of vibrissa units in the anesthetized animal[45]. It measures the bias in the activity of neurons as a vibrissa is deflected in different directions. Notably, directional tuning forms a fine-scale map within a cortical column[46].

Directional tuning may be derived from an asymmetry in the phase preference of a neuron. With phase tuning for contact defined as $T(\phi-\phi_{\text{touch}})$ (Figs. 3d, 4b and Fig. 6), the directional tuning along the anterior-posterior axis is

$$D(\phi_{\text{touch}})=\frac{2\int_{-\pi}^{0} d\phi\{T(\phi-\phi_{\text{touch}})\}_{\text{odd}}}{\int_{-\pi}^{0} d\phi\{T(\phi-\phi_{\text{touch}})\}_{\text{even}}}$$

where odd and even refer to the odd and even parts of the function. The directional tuning is double-valued over the whisk cycle, so that the phase preference of a neuron cannot be uniquely determined from its directional preference. Nonetheless, to the extent that active and passive touch lead to neuronal responses with similar directional preference, neurons with different preferred phases in the whisk cycle are expected to conform to the map for directional tuning.

METHODS

Training and behavior

We successfully trained nine female Long-Evans rats (Charles River), 270 to 300 g initial weight, to whisk against a piezoelectric sensor (DT1–028K; Measurement Specialties Inc.) in return for a liquid food reward (0.2 ml per trial; LD–100; PMI Feeds). We used two behavioral paradigms. In the ‘free ranging’ paradigm (Fig. 1a), we trained unconstrained animals to perch on the edge of a platform and crane their necks to gain access to the sensor. Each trial was initiated when the rat first contacted the sensor. We collected video images at

a frame rate of ~100 frames per second while the rat palpated the sensor to confirm that the longest vibrissa touched the sensor. After an approximately 3-s period of palpation, the trial was terminated by removal of the sensor and concomitant pumping of the liquid reward to a nearby well on the platform. The sensor remained retracted for 5s, then was restored to its previous position so that a new trial could begin. In the 'body constrained' paradigm (Fig. 1b), we placed the animals in a sack and held them in a tube within proximity of a sensor. A trial began when an animal craned and initially touched the sensor and, as above, was terminated after a 3-s period of touch events.

Successful learning of either of the above behaviors took about two weeks. Once training was completed, a small chamber that contained an array of 2 to 4 stereotrodes was fit over the vibrissa area of parietal cortex and secured to the skull with screws and dental acrylic[20]. We individually advanced the stereotrodes through the dura into cortex with a vacuum insertion technique that prevented damage to the upper layers[20]. We threaded fine wires into the left and right mystacial pads to record the EMG[13]. The care and experimental manipulation of our animals were in strict accord with guidelines from the US National Institutes of Health and have been reviewed and approved by the Institutional Animal Care and Use Committee of the University of California, San Diego.

After several days of post-operative recovery, we briefly anesthetized the animals and individually stimulated each contralateral vibrissa with a brief air puff[47] in order to determine the principal vibrissa response for each stereotrode. The designation of the principal vibrissa was based on the amplitude and latency of the stimulus-locked spikes[48]. Once we determined the principal vibrissae across the full complement of stereotrodes, we trimmed all other vibrissae at ~1 mm from the surface of the skin. The rats were returned to their behavioral setup and invariably performed the task with the single, longest vibrissa. We then acquired spiking data with the electrode that had this vibrissa as its principal vibrissa; the electrode was lowered at the start of each recording session by 80 μm, or until single unit spikes were detected. Once this electrode had been lowered through the full depth of cortex, we trimmed the longest vibrissa and proceeded to take data from the next longest vibrissa, and so forth.

Estimation of electrode depth

We exploited the stereotypic form of the radial current source density to identify the lamina of each recording. After all electrodes were lowered through the cortex and data collection was completed, the rat was anesthetized with 5% (w/v) halothane. All electrodes were fully retracted, then lowered in increments of 80 mm while air puffs were delivered at 1.3 puffs per second to passively stimulate all of the vibrissae. We recorded the local field potential at each depth as an average over 100 air puffs[16]. The second spatial derivative was then calculated across all of the averaged local field potential responses to produce an estimate of the one-dimensional current source density profile for each electrode. Current sinks corresponded to the afferent inputs in layers 4 and 6A; these calibration data allowed us to specify the lamella and depth of every record (Fig. 2g and Supplementary Fig. 6).

Data acquisition

Continuous time series from the cortical and EMG microwires were band-pass filtered from 0.35Hz (1 pole) to 10kHz (6 poles), and the piezoelectric sensor was band-pass filtered from 4 kHz (2 poles) to 8 kHz (2 poles). We sampled all data at 32 kHz and stored blocks of approximately 3 s in duration that incorporated each epoch of touch on computer disk, together with the time-locked video images. We obtained additional spike-train records, 10 s in length, as animals were coaxed to whisk in air without contact by placing their home cage just out of reach[16]. We digitally high-pass filtered the broadband cortical and EMG signals

at 300 Hz (4 poles). Pairs of EMG signals that spanned the mystacial pad were subtracted to form the ∇EMG13.

We collected high-speed videography (ES310 charge coupled device camera; Kodak, Inc.) acquired at 100 frames per second during trials where rats contacted the touch sensor with their vibrissae. Synchronization between video and electrophysiological data acquisition was accomplished through a hardware trigger on the Real-Time System Integration Bus (National Instruments). We calculated the angular position of the principal vibrissa on a frame-by-frame basis as the angle between one straight line that followed the midline of the snout and another straight line that followed the first 6 to 10 mm of the vibrissa shaft (Fig. 1c). The lines were drawn manually, for each frame, with the aid of a Matlab (The Mathworks)-based graphical user interface.

Data analysis

An offline non-Gaussian cluster analysis algorithm[21] was used to isolate spikes from an apparent common source in each cortical signal. We characterized modulation of the spike rate of single units during epochs of rhythmic whisking in air, which occurred before and after contact trials, by cross-correlating ∇EMG peak times with spike times. This method allowed us to normalize the correlation in terms of spike rate. We first band-pass filtered the rectified ∇EMG from 3 to 22 Hz and set an appropriate threshold for the signal as a means to isolate the interval that surrounded the peak of the waveform, then calculated the center of mass in these intervals to obtain a point process that represents the peaks of the ∇EMG. We then shifted this time series by 20 ms to account for the measured time delay between the onset of muscle activity, as measured by the ∇EMG, and movement of the vibrissae[13]. The resultant cross-correlation corresponds to the ∇EMG-triggered average spiking rate (Fig. 2a–d, gray histograms in left column, and Fig. 4a). The sinusoidal nature of the cross-correlation was characterized by Poisson-distributed maximum likelihood estimates (MLE) of the mean spike counts[49] for a series of complex exponential functions that spanned the frequency range of 5 to 20 Hz, plus a constant term (function glmfit in Matlab with the log-link function). The frequency of the modulation was defined as the estimate with the highest likelihood among all of the complex exponential estimates in the series. We calculated the phase and amplitude of each response from the real and imaginary parts of the estimate. Finally, we normalized the cross-correlations in terms of spike rates by multiplying the spike counts in each bin by the width of the bin (2 ms) and dividing by the number of ∇EMG peaks in the average (Fig. 2a–d, gray histograms in left column, and Fig. 3a). We used sampling distributions of maximum likelihood estimators to construct 95% confidence intervals of the mean spike rate and parameter estimates.

We estimated touch responses from contact-triggered averages, either across all trials (Fig. 2a – d, gray histograms in middle column, and Fig. 3b) or first parsed according to the phase of whisking at the time of contact (Fig. 3b, gray histograms). Smoothed values for all estimates made use of the Poisson-distributed Bayesian adaptive regression splines nonparametric smoothing algorithm[50] (http://lib.stat.cmu.edu/~kass/bars).

We determined the phases of touch events within the whisk cycle by fitting a series of complex exponentials to the band-pass filtered ∇EMG or to spline-interpolated videographic traces, centered in a 200-ms window that surrounded the time of vibrissa touch. The procedure was as described above for spike events, except that we now used a Gaussian- rather than Poisson-distributed MLE, as the ∇EMG data are a continuous function rather than a point process. We quantified goodness of fit by calculating the ratio of the amplitude of the fit relative to the r.m.s. residual of the fit; we discarded contact events with ratios less than two.

To assess the touch responses as a function of phase in the whisk cycle, cycles in which touch occurred were first divided into eight intervals of π/4 radians. We then binned touch responses according to the interval in which the touch events occurred to produce a set of eight histograms for each single unit (Figs. 3c and 5a,e). To ensure that our results were statistically reliable across the full range of phase intervals, we excluded sessions with less than eight touch events in any phase interval. We then modeled touch responses for each whisk cycle phase interval with a Poisson-distributed MLE as scaled versions of the overall touch response, computed as described above (Fig. 3c–e, red and black curves). We used the peak amplitudes for each of the best fits to construct the tuning curve for the single unit (Figs. 3d and 5b). We calculated confidence intervals (95%) for mean spike rates from sampling distributions of maximum likelihood estimators. A similar procedure was followed to assess the touch responses as a function of angle in the whisk cycle, for which videographic data were used to determine vibrissa position relative to the midline (Fig. 1c).

Model

The circuit model (Fig. 7a) consists of three compartments with equal membrane capacitances, C, and resistances, R, that are joined by a resistance of R so that the compartments are one electrotonic length apart in the absence of synaptic input. We define E_L, E_B, E_S and E_E as the reversal potentials for the leak, excitatory bias, inhibitory synaptic shunt and excitatory synaptic currents, respectively, G_L as the fixed leak conductance, G_B as the conductance of a slowly varying bias current, and G_S and G_E as the conductances for the vibrissa-driven inhibitory shunt and touch-driven excitation, respectively. For constant values of the conductances, the steady state subthreshold voltage of the active zone, denoted V_m, is given by:

$$V_\mathrm{m}=\frac{(8+2RG_S+4RG_E+RG_SRG_E)E_L+RG_B(5+2RG_S+3RG_E+RG_SRG_E)+E_B+RG_S(2+RG_E)E_S+RG_EE_E}{8+5RG_B+2(2+RG_B)RG_S+(5+3RG_B)+RG_E+(2+RG_B)RG_SRG_E} \tag{4}$$

The full dynamics are found by solving five equations, which include a third-order Hindmarsh-Rose system to generate spikes in a cortical cell with adaptation, and additive band-limited Gaussian noise to approximate the variability in synaptic arrival time. We have

$$\frac{dV_\mathrm{m}}{dt}=\frac{1}{\tau_\mathrm{m}}\left\{(a+bV_\mathrm{m}+cV_\mathrm{m}^2)(E_\mathrm{Na}-V_\mathrm{m})+RG_R(E_K-V_\mathrm{m})U+RG_A(E_K-V_\mathrm{m})W+RG_B(E_\mathrm{B}-V_\mathrm{m})+(V_\mathrm{s}-V_\mathrm{m})+I_\mathrm{noise}\right\} \tag{5}$$

$$\frac{dU}{dt}=\frac{1}{\tau_U}\left\{-U+eV_\mathrm{m}+f+g(E_{KA}-V_\mathrm{m})^2\right\} \tag{6}$$

$$\frac{dW}{dt}=\frac{1}{\tau_W}\{-W+h(E_1-V_\mathrm{m})(E_2-V_\mathrm{m})\} \tag{7}$$

$$\frac{dV_S}{dt}=\frac{1}{\tau_m}\{(E_S-V_S)RG_S+(E_L-V_S)RG_L+(V_\mathrm{m}-V_S)+(V_E-V_S)\} \tag{8}$$

$$\frac{dV_E}{dt} = \frac{1}{\tau_m}\{(E_E - V_E)RG_E + (E_L - V_E)RG_L + (V_S - V_E)\} \tag{9}$$

where the leak term $RG_L(E_L - V_m)$ in the dynamics for V_m is subsumed in the active currents, and τ_m = 1 ms, τ_U = 1 ms, τ_W = 99 ms, E_{Na} = 48 mV, E_K = –95 mV, E_{KA} = −38 mV, E_S = E_L = −74 mV, E_B = E_E = +10 mV, E_1 = −75.4 mV, E_2 = −69 mV, RG_R = 26, RG_A = 13, RG_B = 0.2 (ranges 0.05 to 0.8), RG_L = 1, a = 17.8, b = 0.476 mV^{-1}, c = 3.38 × 10^{-3} mV^{-2}, e = 1.3 × 10^{-2}, f = 0.8, g = 3.3 × 10^{-4} and h = 1.1 × 10^{-3} in our simulations. The noise current has an r.m.s. value of 2.0 mV; the shunting inhibitory conductance was of the form

$$RG_S = \frac{RG_{SO}}{2}\{1 + \cos(2\pi f_{\text{whisk}} t - \phi_{\text{whisk}})\} \tag{10}$$

where RG_{SO} = 10 (ranges 0 to 20) and f_{whisk} = 9Hz; and the excitatory touch conductance was of the form

$$RG_E = RG_{EO} e^{-(t - t_{EO})^2 / 2\tau_{EO}^2} \tag{11}$$

where RG_{EO} = 40, τ_{EO} = 20 ms and t_{EO} is a random variable with a mean of 0.25 s that marks touch events.

Supplementary Material

Refer to Web version on PubMed Central for supplementary material.

Acknowledgments

We thank S.B. Mehta for assistance with spike sorting, E.N. Brown and R.E. Kass for instruction on spike-train analysis, G.A. White for electronics support, E. Ahissar, W. Denk, M. Deschenes, M.E. Diamond, A.L. Fairhall, D.N. Hill and T.J. Sejnowski for relevant discussions, D. Matthews for reading of the manuscript, and the US National Institutes of Health (NS051177), the US National Science Foundation (IGERT) and the US/Israel Binational Foundation (2003222) for financial support.

References

1. von Holst E. Relations between the central nervous system and the peripheral organ. Br. J. Anim. Behav 1954;2:89–94.
2. Cullen KE. Sensory signals during active versus passive movement. Curr. Opin. Neurobiol 2004;14:698–706. [PubMed: 15582371]
3. Sommer MA, Wurtz RH. Influence of the thalamus on spatial visual processing in frontal cortex. Nature 2006;444:374–377. [PubMed: 17093408]
4. Roy JE, Cullen KE. Dissociating self-generated from passively applied head motion: neural mechanisms in the vestibular nuclei. J. Neurosci 2004;24:2102–2111. [PubMed: 14999061]
5. Lal R, Friedlander MJ. Effect of passive eye position changes on retinogeniculate transmission in the cat. J. Neurophysiol 1990;63:502–522. [PubMed: 2329358]
6. Ashton JA, Boddy A, Donaldson IM. Directional selectivity in the responses of units in cat primary visual cortex to passive eye movement. Neuroscience 1984;13:653–662. [PubMed: 6527771]
7. Andersen RA, Snyder LH, Li CS, Stricanne B. Coordinate transformations in the representation of spatial information. Curr. Opin. Neurobiol 1993;3:171–176. [PubMed: 8513228]
8. Mehta SB, Whitmer D, Figueroa R, Williams BA, Kleinfeld D. Active spatial perception in the vibrissa scanning sensorimotor system. PLoS Biol 2007;5:e15. [PubMed: 17227143]

9. Deschenes M, Timofeeva E, Lavallée P, Dufresne E. The vibrissal system as a model of thalamic operations. Prog. Brain Res 2005;149:31–40. [PubMed: 16226574]
10. Fox, K. Barrel Cortex. Cambridge: Cambridge University Press; 2008. p. 14-48.
11. Kleinfeld D, Berg RW, O'Connor SM. Anatomical loops and their electrical dynamics in relation to whisking by rat. Somatosens. Mot. Res 1999;16:69–88. [PubMed: 10449057]
12. Ahissar E, Kleinfeld D. Closed loop neuronal computations: focus on vibrissa somatosensation in rat. Cereb. Cortex 2003;13:53–61. [PubMed: 12466215]
13. Berg RW, Kleinfeld D. Rhythmic whisking by rat: retraction as well as protraction of the vibrissae is under active muscular control. J. Neurophysiol 2003;89:104–117. [PubMed: 12522163]
14. Szwed M, Bagdasarian K, Ahissar E. Coding of vibrissal active touch. Neuron 2003;40:621–630. [PubMed: 14642284]
15. Fee MS, Mitra PP, Kleinfeld D. Central versus peripheral determinates of patterned spike activity in rat vibrissa cortex during whisking. J. Neurophysiol 1997;78:1144–1149. [PubMed: 9307141]
16. Ganguly K, Kleinfeld D. Goal-directed whisking behavior increases phase-locking between vibrissa movement and electrical activity in primary sensory cortex in rat. Proc. Natl. Acad. Sci. USA 2004;101:12348–12353. [PubMed: 15297618]
17. Crochet S, Petersen CCH. Correlating membrane potential with behaviour using whole-cell recordings from barrel cortex of awake mice. Nat. Neurosci 2006;9:608–609. [PubMed: 16617340]
18. Yu C, Derdikman D, Haidarliu S, Ahissar E. Parallel thalamic pathways for whisking and touch signals in the rat. PLoS Biol 2006;4:e124. [PubMed: 16605304]
19. Pierret T, Lavallee P, Deschenes M. Parallel streams for the relay of vibrissal information through thalamic barreloids. J. Neurosci 2000;20:7455–7462. [PubMed: 11007905]
20. Venkatachalam S, Fee MS, Kleinfeld D. Ultra-miniature headstage with 6-channel drive and vacuum-assisted micro-wire implantation for chronic recording from neo-cortex. J. Neurosci. Methods 1999;90:37–46. [PubMed: 10517272]
21. Fee MS, Mitra PP, Kleinfeld D. Automatic sorting of multiple unit neuronal signals in the presence of anisotropic and non-Gaussian variability. J. Neurosci. Methods 1996;69:175–188. [PubMed: 8946321]
22. Simons DJ. Response properties of vibrissal units in rat S1 somatosensory neocortex. J. Neurophysiol 1978;41:798–820. [PubMed: 660231]
23. Mountcastle VB, Talbot WH, Sakata H, Hyvarinen J. Cortical neuronal mechanisms in flutter-vibration studied in unanesthetized monkeys, neuronal periodicity and frequency discrimination. J. Neurophysiol 1968;32:452–484. [PubMed: 4977839]
24. Krupa DJ, Wiest MC, Shuler MG, Laubach M, Nicolelis MA. Layer-specific somatosensory cortical activation during active tactile discrimination. Science 2004;304:1989–1992. [PubMed: 15218154]
25. Bartho P, et al. Identification of neocortical principal cells and interneurons by extracellular features. J. Neurophysiol 2004;92:600–608. [PubMed: 15056678]
26. Derdikman D, et al. Layer-specific touch-dependent facilitation and depression in the somatosensory cortex during active whisking. J. Neurosci 2006;26:9538–9547. [PubMed: 16971538]
27. Olson CR. Brain representation of object-centered space in monkeys and humans. Annu. Rev. Neurosci 2003;26:331–354. [PubMed: 12626696]
28. Leiser SC, Moxon KA. Responses of trigeminal ganglion neurons during natural whisking behaviors in the awake rat. Neuron 2007;53:117–133. [PubMed: 17196535]
29. Arvidsson J, Rice FL. Central projections of primary sensory neurons innervating different parts of the vibrissae follicles and intervibrissal skin on the mystacial pad of the rat. J. Comp. Neurol 1991;309:1–16. [PubMed: 1716645]
30. Maravall M, Petersen RS, Fairhall AL, Arabzadeh E, Diamond ME. Shifts in coding properties and maintenance of information transmission during adaptation in barrel cortex. PLoS Biol 2007;5:e19. [PubMed: 17253902]

31. Urbain N, Deschênes M. A new thalamic pathway of vibrissal information modulated by the motor cortex. J. Neurosci 2007;27:12407–12412. [PubMed: 17989305]
32. Masri R, Bezdudnaya T, Trageser JC, Keller A. Encoding of stimulus frequency and sensor motion in the posterior medial thalamic nucleus. J. Neurophysiol 2008;100:681–689. [PubMed: 18234976]
33. McCormick DA, Connors BW, Lighthall JW, Prince DA. Comparative electro-physiology of pyramidal and sparsely spiny stellate neurons of the neocortex. J. Neurophysiol 1985;54:782–806. [PubMed: 2999347]
34. Ahrens KF, Levine H, Suhl H, Kleinfeld D. Spectral mixing of rhythmic neuronal signals in sensory cortex. Proc. Natl. Acad. Sci. USA 2002;99:15176–15181. [PubMed: 12403828]
35. Pena JL, Konishi M. Robustness of multiplicative processes in auditory spatial tuning. J. Neurosci 2004;24:8907–8910. [PubMed: 15470157]
36. Andersen RA, Mountcastle VB. The influence of angle of gaze upon the excitability of the light sensitive neurons of the posterior parietal cortex. J. Neurosci 1983;3:532–548. [PubMed: 6827308]
37. Salinas E, Abbott LF. A model of multiplicative neural responses in parietal cortex. Proc. Natl. Acad. Sci. USA 1996;93:11956–11961. [PubMed: 8876244]
38. Koch C, Poggio T, Torre V. Nonlinear interactions in a dendritic tree: localization, timing, and role in information processing. Proc. Natl. Acad. Sci. USA 1983;80:2799–2802. [PubMed: 6573680]
39. Richardson MJ, Brunel N, Hakim V. From subthreshold to firing-rate resonance. J. Neurophysiol 2003;89:2538–2554. [PubMed: 12611957]
40. Rudolph M, Pospischil M, Timofeev I, Destexhe A. Inhibition determines membrane potential dynamics and controls action potential generation in awake and sleeping cat cortex. J. Neurosci 2007;16:5280–5290. [PubMed: 17507551]
41. Lee AK, Manns ID, Sakmann B, Brecht M. Whole-cell recordings in freely moving rats. Neuron 2006;51:399–407. [PubMed: 16908406]
42. de Kock CP, Bruno RM, Spors H, Sakmann B. Layer- and cell-type-specific suprathreshold stimulus representation in rat primary somatosensory cortex. J. Physiol. (Lond.) 2007;581:139–154. [PubMed: 17317752]
43. Manns ID, Sakmann B, Brecht M. Sub- and suprathreshold receptive field properties of pyramidal neurones in layers 5A and 5B of rat somatosensory barrel cortex. J. Physiol. (Lond.) 2004;556:601–622. [PubMed: 14724202]
44. Knutsen PM, Pietr M, Ahissar E. Haptic object localization in the vibrissal system: behavior and performance. J. Neurosci 2006;26:8451–8464. [PubMed: 16914670]
45. Bruno RM, Khatri V, Land PW, Simons DJ. Thalamocortical angular tuning domains within individual barrels of rat somatosensory cortex. J. Neurosci 2003;19:7603–7616.
46. Andermann ML, Moore CI. A somatotopic map of vibrissa motion direction within a barrel column. Nat. Neurosci 2006;9:543–551. [PubMed: 16547511]
47. Kleinfeld D, Sachdev RNS, Merchant LM, Jarvis MR, Ebner FF. Adaptive filtering of vibrissa input in motor cortex of rat. Neuron 2002;34:1021–1034. [PubMed: 12086648]
48. Armstrong-James M, Fox K, Das-Gupta A. Flow of excitability within barrel cortex on striking a single vibrissa. J. Neurophysiol 1992;68:1345–1358. [PubMed: 1432088]
49. Brown EN, Frank LM, Tang D, Quirk MC, Wilson MA. A statistical paradigm for neural spike train decoding applied to position prediction from ensemble firing patterns of rat hippocampal place cells. J. Neurosci 1998;18:7411–7425. [PubMed: 9736661]
50. DiMatteo I, Genovese CR, Kass RE. Bayesian curve-fitting with free-knot splines. Biometrika 2001;88:1055–1071.

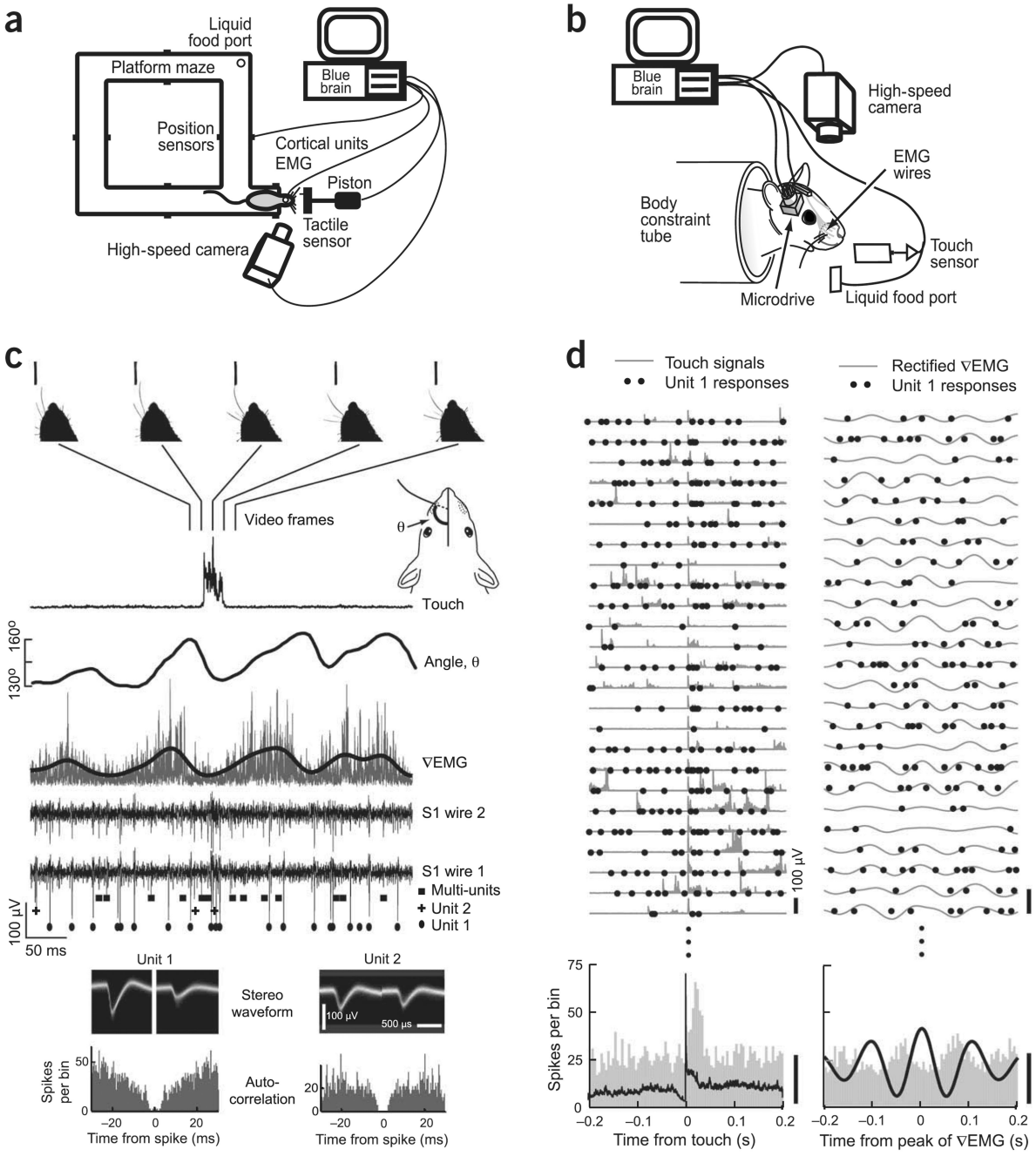

Figure 1.

Experimental setups and data acquisition. (**a**) Free ranging apparatus. The rat cranes from a perch to contact a piezoelectric touch sensor that is held in position by a pneumatic piston and imaged with a high-speed camera. Five seconds after the initial contact the sensor is withdrawn and the rat receives a liquid food reward. Spike signals from stereotrodes in the rat's cortex and EMG electrodes in the mystacial pad, along with contact, positional and video data, are logged. (**b**) Body restrained apparatus. The animal is wrapped in a sack that is held in a plastic tube. All other experimental features as in **a**, except that food is delivered from a port close to the animal's head. (**c**) Examples of primary data surrounding contact events, including vibrissa position data, the rectified touch signal and accompanying video

frames, the rectified ∇EMG and lowpass filtered rectified ∇EMG, and the neuronal activity from both channels of the stereotrode. We further show the spike times from two single units after sorting of the spike data; the bottom plots show the respective waveforms and autocorrelations. (**d**) The left strip shows the response of unit 1 in **c** to touch across multiple trials, together with the touch signal. The right strip shows the response during free whisking, together with the concurrent ∇EMG. The averages relative to contact and to the peak of the ∇EMG signals are shown at the bottom of the panel.

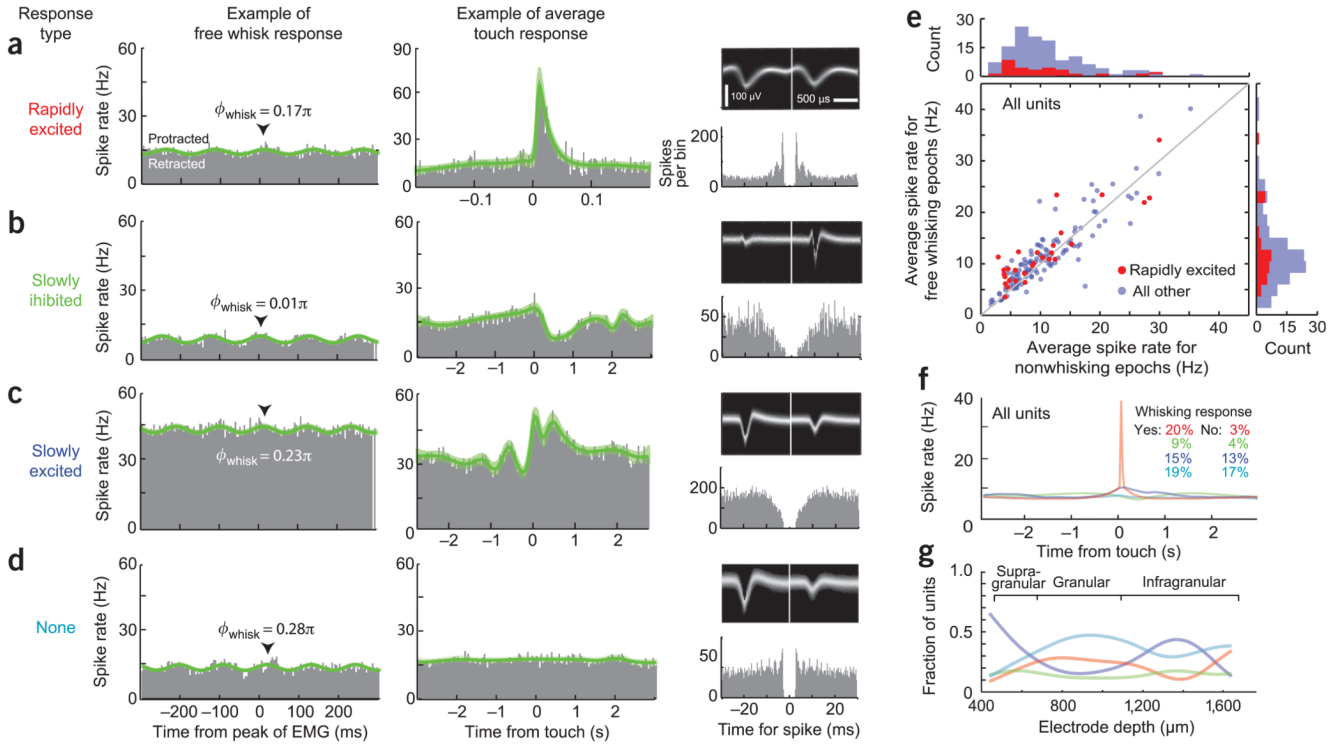

Figure 2.

Free whisking and exemplar touch responses of all single units. (**a–d**) Spike rates for rapidly excited (**a**), slowly inhibited (**b**), slowly excited (**c**) and no (**d**) response. The left column is a histogram of the average spike rate centered on the peaks of ∇EMG activity, which corresponds to the maximal protraction. Spike rates were fit with Poisson maximum likelihood estimates of a series of complex exponentials to determine the baseline firing rate and the dominant whisking frequency, amplitude and phase of each spike response (green line). The phase for the peak response is defined as ϕ_{whisk}. The middle column is a histogram of the touch response, smoothed using Bayesian adaptive regression splines (green line). The last column shows the temporal waveform and autocorrelation function for the unit. The uncertainly in all cases is represented by 95% confidence intervals. (**e**) The spike rate for all units whose spike rate was significantly ($P < 0.05$) modulated by whisking versus the rate in the absence of whisking; in neither case did the vibrissae contact an object. A fit to the data of $Rate_{whisking} = slope \times Rate_{nonwhisking}$ yields slope = 1.05 ± 0.11 (mean ± 2 s.e.m.) for rapidly excited units and slope = 1.03 ± 0.04 for all other units; neither slope is significantly different from unity (line). (**f**) Average response to touch over all single units in a given class of both whisking and touch-sensitive units. The compendium is the percent of total responses across all single units. (**g**) The laminar distribution of single units that responded to active touch, independent of their whisking-related response (Supplementary Fig. 6).

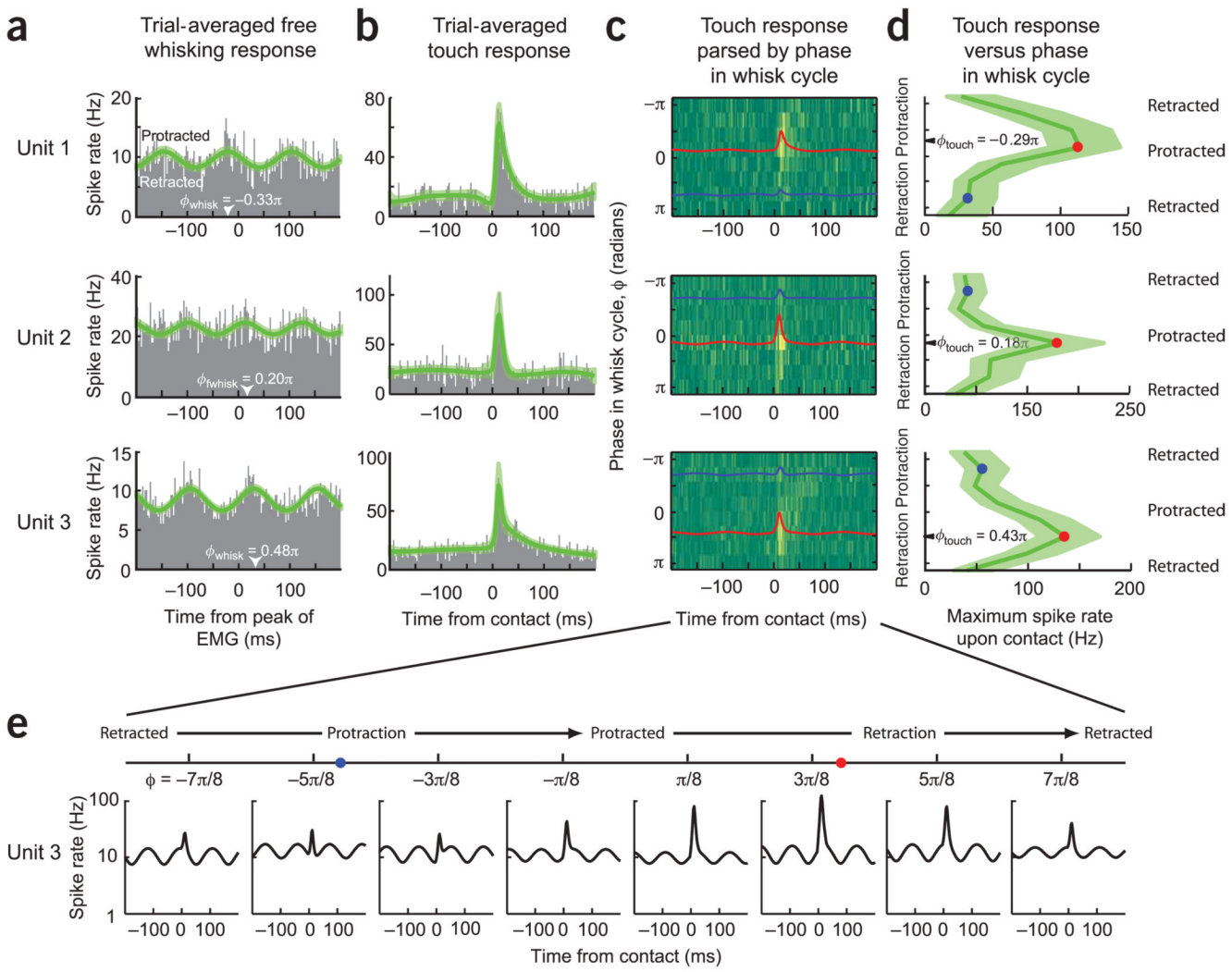

Figure 3.

Examples of the interaction between phase in the whisk cycle, as determined from the ∇EMG signal, and the response of rapidly excited touch-sensitive single units. (**a**) Histograms of the spike responses to free whisking in air. The spike rates were fit with sinusoids (green line). (**b**) Histograms of the touch response, averaged over all events, as a function of time from the measured contact. The spike rates were fit with smooth curves (green line). (**c**) Histograms of the touch response parsed according to the phase in the whisk cycle upon contact. The phase interval is π/4 radians. The red curves correspond to the interval with the maximum response, and the black curves correspond to a lower response; these curves are scaled versions of smoothed trial-averaged touch responses in **b**. (**d**) Plots of the peak values of the touch response from the fits to each of the eight intervals of the touch responses in **c**; dots designate the example fits from **c**. The uncertainty represents the 95% confidence interval. A smooth curve through this data defines the phase of maximal touch response, denoted ϕ_{touch}. (**e**) Curves derived from sinusoid fits of the pre- and post-touch response and smooth curves of the touch response are shown for the data of unit 3 and plotted on a logarithmic scale. The responses to touch events for whisking phases near $\phi = -(5/8)\pi$ are minimal and are close to the trough of the modulation of spiking by whisking.

The touch response increases in amplitude for contact events close to the peak of the modulation of spiking by whisking, that is, near $\phi = (3/8)\pi$.

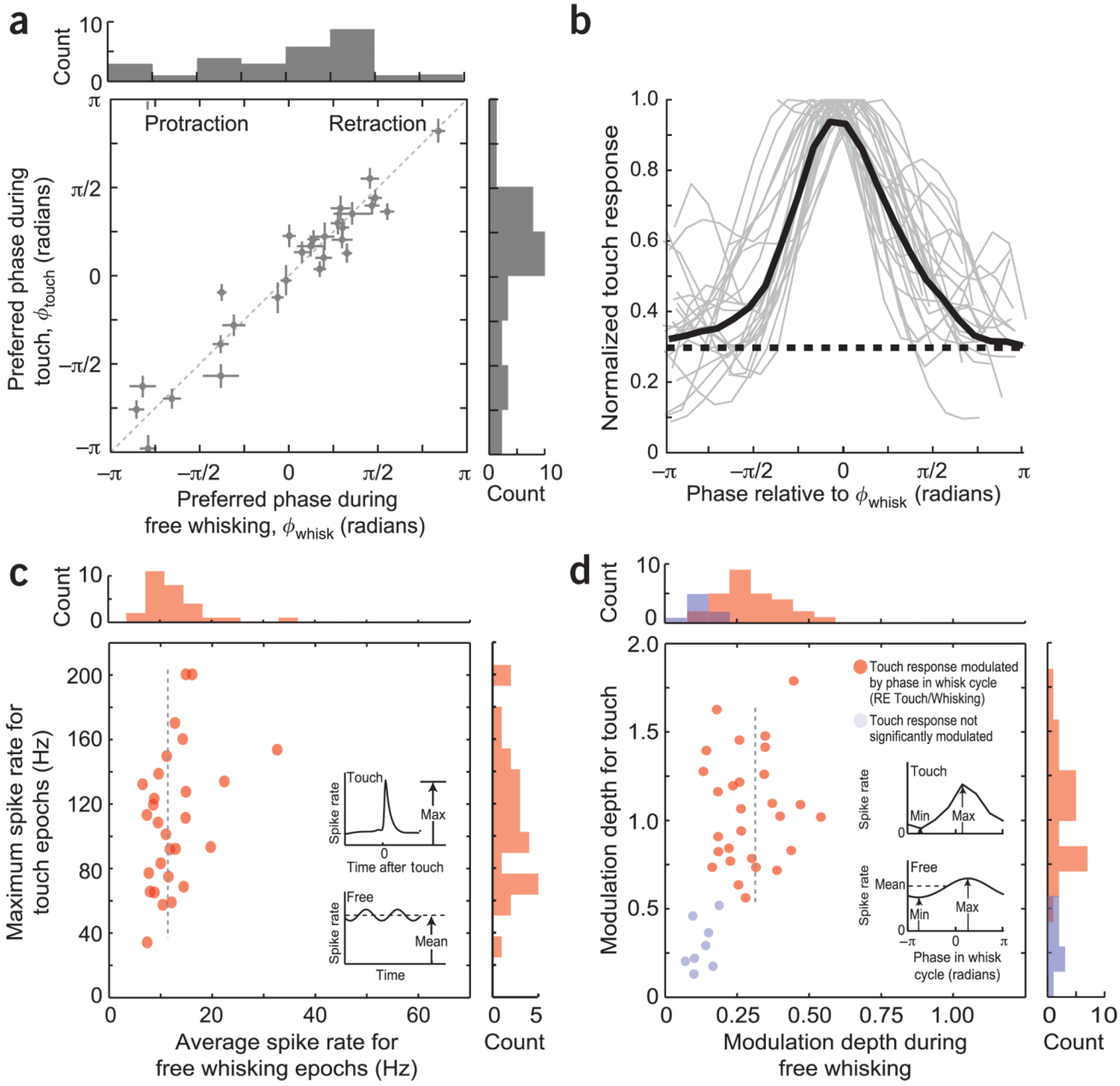

Figure 4.

Summary of the phase sensitivity and spike rate modulation of rapidly excited touch-sensitive single units. (**a**) Scatter plot of the preferred phase for free whisking versus the preferred phase for touch. Shown are mean values plus 95% confidence intervals for the estimates of either phase. The data are consistent with $\phi_{touch} = \phi_{whisk}$ ($P < 0.001$). (**b**) Touch responses as a function of phase in the whisk cycle (gray), where each curve is normalized to its peak value and centered with respect to ϕ_{whisk}, the preferred phase for the unit while the rat whisked in air. The solid black curve is the population average, and the dashed curve is the minimum relative spike activity. (**c**) The maximum spike rates during active touch (Max in inset) versus the average spike rates while whisking in air (Mean in inset). (**d**)

Comparison of the modulation depths (equation (1)) of the spike rates for touch versus free whisking.

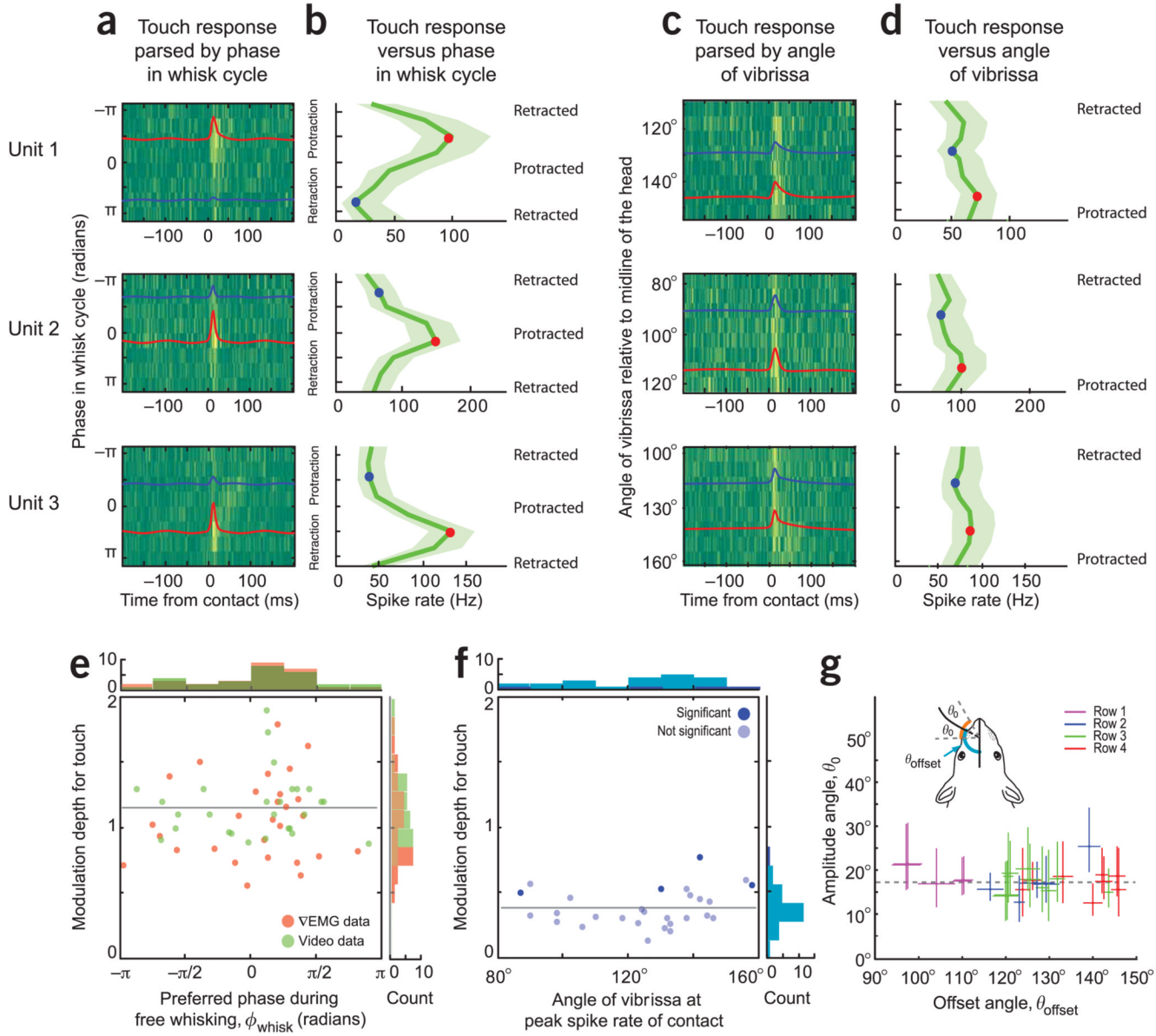

Figure 5.

Comparison of the phase dependence versus angular position dependence of the touch response, derived from videographic analysis of vibrissa position, for rapidly excited touch-sensitive single units. (**a**) Histograms of the touch response parsed according to the phase in the whisk cycle upon contact; phase interval is π/4 radians. The red curves correspond to the interval with the maximum response, and the black curves correspond to a lower response. (**b**) Plots of the peak values of the touch response from the fits to each of the eight intervals of the touch responses in **a**; dots designate the example fits from **a**. The uncertainty represents the 95% confidence interval. A smooth curve through this data defines the phase of maximal touch response. (**c**) Histograms of the touch response parsed according to the angular position of the vibrissa upon contact. The angle relative to the midline of the animal's head was determined from videographic analysis of vibrissa position (Fig. 1c). The red curves correspond to the interval with the maximum response, and the black curves correspond to a lower response. (**d**) Plots of the peak values of the touch response from the

fits to each of the eight intervals of the touch responses in **c**; dots designate the example fits from **c**. (**e**) Comparison of the modulation depths (equation (1)) of the spike rates for touch versus phase in the whisk cycle. We show the data with phase determined from videography (green) and phase determined from the ∇EMG (red; Fig. 4d). All points are significantly ($P < 0.05$) modulated. (**f**) Comparison of the modulation depths (equation (1)) of the spike rates for touch versus angular position in the whisk cycle. Only 4 of 28 points are significantly ($P < 0.05$) modulated. (**g**) The angular amplitude (orange arcs) and midpoint (blue arc) for whisking for each of the RE touch-sensitive single units. The bars denote the 95% range of variation of parameters across all trials.

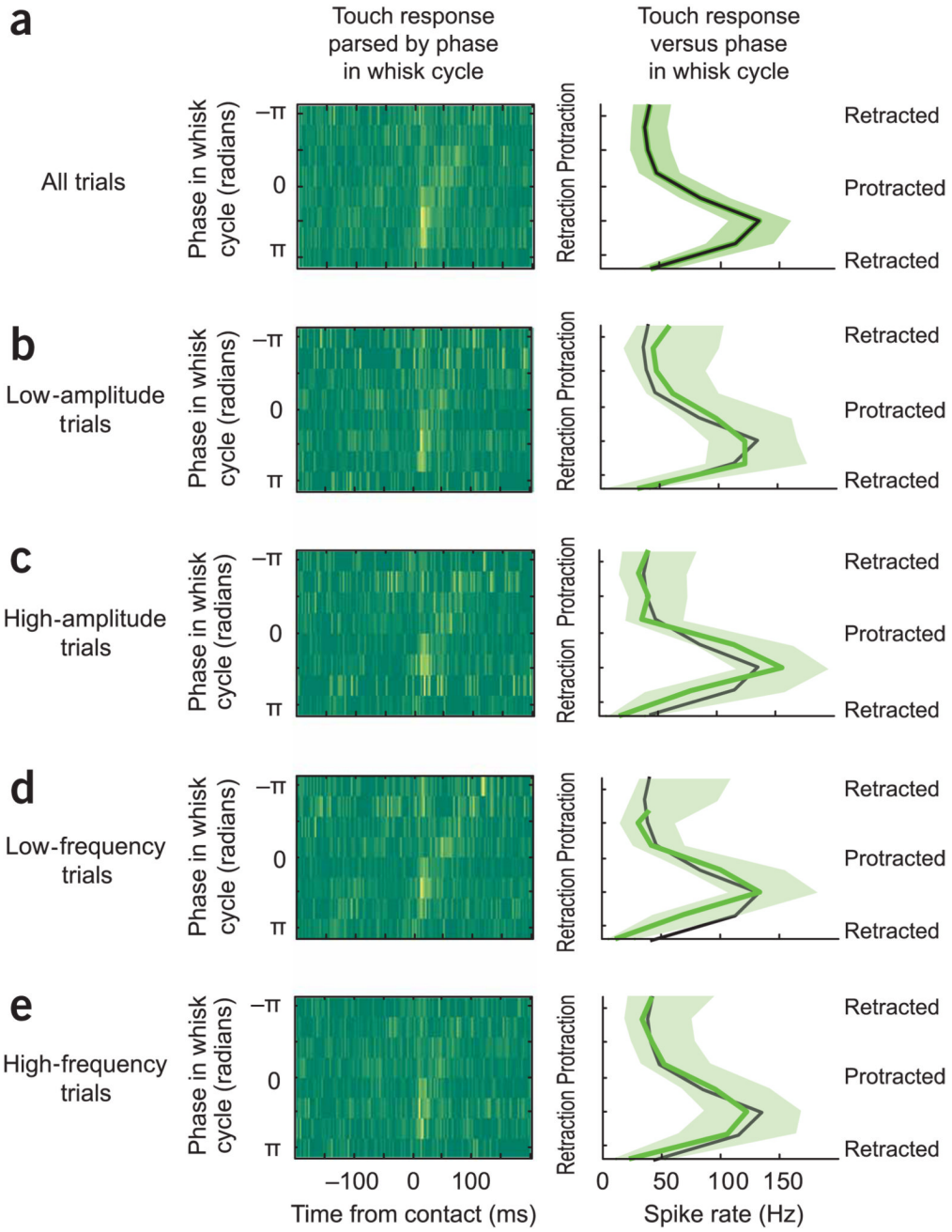

Figure 6.

Example of the phase dependence as a function of whisking parameters for a rapidly excited touch-sensitive single unit. (**a**) The response for unit 3 (Figs. 3 and 5) averaged over all trials, for which $\phi_{whisk} = 0.45\ \pi$. (**b,c**) The touch response for unit 3 parsed according to the angular position of the vibrissa upon contact and separated into low-amplitude (4° to 12°, **b**) versus large-amplitude (13° to 25°, **c**) whisks, with preferred phases $\phi_{whisk} = 0.46\pi$ and $\phi_{whisk} = 0.38\pi$, respectively. The black curve is the combined response from **a**. (**d,e**) The touch response for unit 3 parsed according to the frequency of whisking and separated into low-frequency (5 to 9Hz, **d**) versus high-frequency (10 to 13 Hz, **e**) whisks, with preferred phases $\phi_{whisk} = 0.37\pi$ and $\phi_{whisk} = 0.40\pi$, respectively.

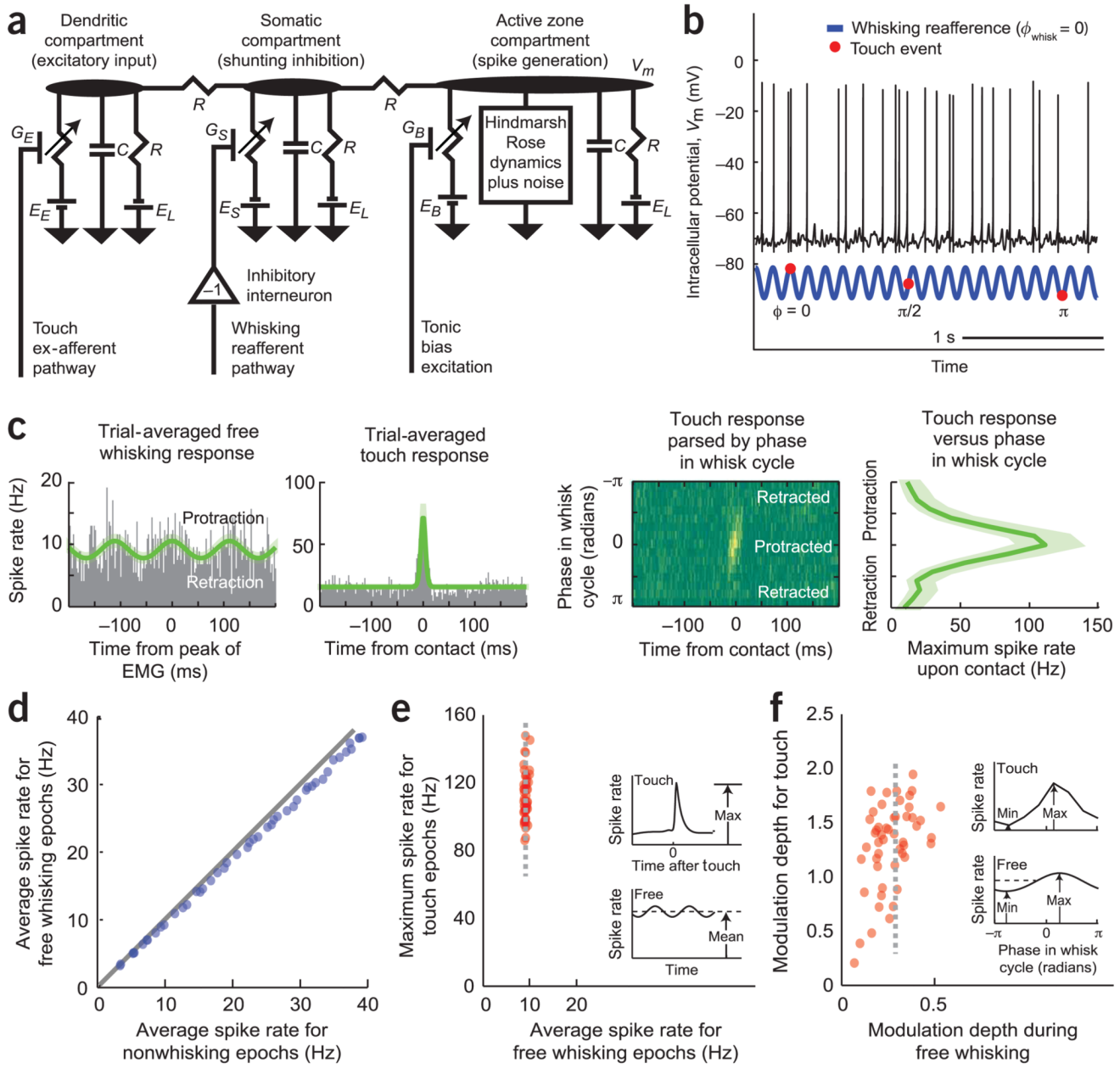

Figure 7.

Shunting-inhibition model for the phase sensitivity of active touch. (**a**) Circuit diagram for the three-compartment neuron that captures the essence of shunting inhibition. The whisking signal is 'inverted' by a local inhibitory neuron and acts as a shunt between distal excitatory touch input and the soma. (**b**) Example results from a numerical simulation of the circuit equation for our model; note the extra spike for 'touch' near the preferred phase of ϕ_{whisk} = 0. (**c**) Example result for one model neuron. The same analysis tools were used as with the data for RE/touch units (Fig. 4). The left column is a histogram of the average spike rate centered on the peaks of EMG activity, corresponding to protraction. The next two columns are histograms of the touch response, shown as a composite and by phase in the whisk cycle. The right column shows the tuning curve. (**d**) The trial-averaged maximal spike rates during

active touch versus the average spike rates while whisking in air; $0.05 < RG_B < 0.8$. (**e**) The maximum spike rate upon contact versus the mean rate; $0 < RG_{SO} < 20$ (equation (10)). (**f**) The modulation depth of the spike rate as a function of phase in the whisk cycle versus the modulation with phase in the whisk cycle; $0 < RG_{SO} < 20$.